Lab on a Chip

Accepted Manuscript

ROYAL SOCIETY OF CHEMISTRY

www.rsc.org/loc

Table of Contents Entry – "Reconfigurable Microfluidics with Integrated Aptasensors for Monitoring Intercellular Communication" by Kwa et al.

We report the development of a microsystem integrating anti-TNF-α aptasensors with vacuum-actuatable microfluidic devices for monitoring intercellular communications.

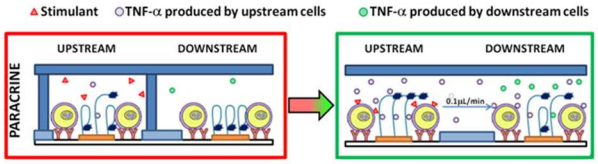

Cite this: DOI: 10.1039/c0xx00000x

www.rsc.org/xxxxxx

ARTICLE TYPE

Reconfigurable Microfluidics with Integrated Aptasensors for Monitoring Intercellular Communication

Timothy Kwa[a], Qing Zhou[a], Yandong Gao[a], Ali Rahimian[a], Lydia Kwon[a], Ying Liu[a] and Alexander Revzin*[a]

Received (in XXX, XXX) XthXXXXXXXXX 20XX, Accepted Xth XXXXXXXXX 20XX
DOI: 10.1039/b000000x

We report the development of a microsystem integrating anti-TNF-α aptasensors with vacuum-actuatable microfluidic devices that may be used to monitor intercellular communications. Actuatable chambers were used to expose to mitogen a group of ~600 cells while not stimulating another group of monocytes only 600μm away. Co-localizing groups of cells with miniature 300μm diameter aptamer-modified electrodes enabled monitoring TNF-α release from each group independently. The microsystem allowed to observe the sequence of events that included 1) mitogenic activation of the first group of monocytes to produce TNF-α, 2) diffusion of TNF-α to the location of the second group of cells and 3) activation of the second group of cells resulting in production of TNF-α by these cells. Thus we were able to experimentally verify reciprocal paracrine cross-talk between the two groups of cells secretion the same signalling molecule. Given the prevalence of such cellular communications during injury, cancer or immune response and the dearth of available monitoring techniques, the microsystem described here is envisioned to have significant impact on cell biology.

Introduction

Pro-inflammatory cytokine tumor necrosis factor alpha (TNF-α) has been found to play a vital role in multiple pathological conditions related to inflammation, such as cancer, rheumatoid arthritis, and Crohn's disease[1-3]. Importantly, TNF-α is a ubiquitous inflammatory signal that is produced by a wide variety of cells and that acts in both paracrine and autocrine fashion. The question of injury genesis and cellular origins of inflammatory signalling often arise in biology and are difficult to answer using standard tools. In this paper, we demonstrate how a microsystem integrating microfluidics with biosensors may be used to monitor paracrine communication between two groups of immune cells via secreted TNF-α.

Well-established techniques such as intracellular cell staining flow cytometry[4, 5], the enzyme-linked immunosorbent spot (ELISpot) assay[6, 7], and PCR-based methods[8, 9] have been used for quantifying cytokine production. While robust and widely used, these techniques are in general suboptimal for analysis of cellular interactions and dynamic monitoring of cell function.

Lab-on-a-chip devices allow for precise placement of cells in a well-defined microenvironment and are therefore particularly well-suited for cell analysis experiments. Microfluidic and microfabricated platforms have been used extensively in the development of multiplexed immunoassays for blood analysis[10-13] and in single cell analysis[14-19]. Typically, microdevices assaying cell-secreted factors such as proteins rely on antibodies for detection. However, while specific and sensitive, antibody-based assays are challenging to adapt for monitoring dynamics of cell secretion since each assay can only provide information at a single timepoint. This challenge has been addressed in previous reports by using sophisticated multi-chamber and multi-layer microfluidics[20], employing multiple antibody-coated surfaces sequentially[21], coupling living cells to an SPR instrument[22, 23] or sensing with microring resonators[24]. However, these devices are either technically complicated, expensive, or have a large footprint that limits spatiotemporal resolution required for analysis of cellular interactions.

Aptamer-based biosensors offer an effective alternative to antibody-based detection. One of the most attractive features of aptasensors is the simplicity with which an oligonucleotide may be designed into a beacon emitting optical or electrical signal directly upon analyte binding[25-28]. Recently, our laboratory integrated aptamer-modified electrodes within microfluidic devices for local and continuous detection of IFN-γ and TNF-α secretion of immune cells[29, 30].

In the present study we sought to integrate aptasensors within a reconfigurable microfluidic device that allows the control, on cue, of the cellular microenvironment by raising or lowering microstructured chambers (Figure 1). The glass surfaces containing microfabricated Au electrodes were micropatterned with a nonfouling hydrogel to define several sites for cell attachment. Electrodes were functionalized with aptamer

molecules to create TNF-α specific aptasensors. Upon actuation of the microstructured roof one group of cells became sequestered inside a microcup while the neighbouring group remained in the open channel. This design allowed selective mitogenic activation of one group of monocyte-like cells (U937 cell line) while keeping a neighbouring group of cells quiescent. Integrating miniature TNF-α aptasensors next to each group of cells allowed us to confirm production of this cytokine by activated U937 cells and its diffusion/convection to the site of quiescent cells. Continuous monitoring of the two groups of cells revealed that previously quiescent cells began producing TNF-α molecules of their own in response to inflammatory signals (including TNF-α) secreted by the mitogenically activated cells. The ability to monitor where and when cell-secreted signals originate and how they affect neighbouring cells provides a new means for dissecting paracrine reciprocal signalling that is widely encountered in cancer, cellular development, immune response, and tissue injury.

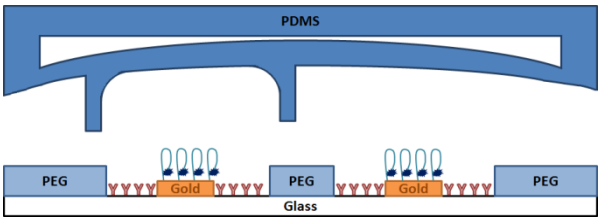

Step 1. Apply vacuum to the upper chamber and incubate TNF-α aptamers followed by CD4 antibodies.

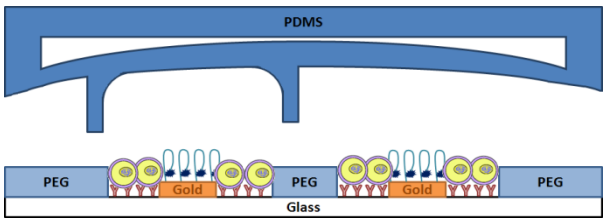

Step 2. Capture immune cells, add stimulant, and release vacuum from the upper chamber to encase some cells (left) within microchambers to limit diffusion.

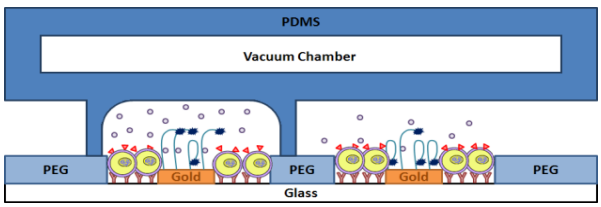

Step 3. Monitor time-resolved cytokine secretion from cells enclosed in a chamber vs. cells in an open environment as a function of electrochemical signal.

Figure 1. Description of the sensing microsystem. Glass substrates were micropatterned so as to contain miniature gold electrodes surrounded by regions for cell adhesion defined in PEG hydrogel layer. This micropatterned surface was then integrated with reconfigurable microfluidics. The microfluidic device was actuated to lower a microcup around a group of cells, creating an 80 nL compartment, increasing concentration of cell secreted cytokines and enhancing the signal. By registering micropatterned surface within a PDMS fluidic channel containing a microstructured membrane, compartments could be created around alternating groups of cells. This allowed selectively activating one group of cells and then monitoring cross-talk between active and quiescent cells via secreted TNF-α.

Materials and Methods

Materials

1×phosphate-buffered saline (PBS) without calcium and magnesium, Na4EDTA, KHCO3, NH4Cl, anhydrous toluene (99.9%), poly(ethylene glycol) diacrylate (PEG-DA, MW 575), dimethyl formamide (DMF), and 2-hydroxy-2-methyl-propiophenone (photoinitiator) were purchased from Sigma-Aldrich (St. Louis, MO). Chromium etchant (CR-4S) and gold etchant (Au-5) were purchased from Cyantek Corporation (Fremont, CA). Positive photoresist (S1813) and developer solution (MIF-319) were purchased from Shipley (Marlborough, MA). 3-Acryloxypropyl trichlorosilane was purchased from Gelest, Inc. (Morrisville, PA). Monoclonal purified mouse anti-human CD4 Abs (clone 13B8.2) were acquired from Beckman-Coulter (Fullerton, CA).Human recombinant TNF-α and interleukin-10 were acquired from R&D Systems (Minneapolis, MN). Monocyte activation reagents: phorbol 12-myristate 13-acetate (PMA) and ionomycin were purchased from Sigma–Aldrich (St. Louis, MO). Cell culture medium RPMI 1640 with L-glutamine without phenol red, qualified fetal bovine serum, and penicillin streptomycin were purchased from Life Technologies (Grand Island, NY). Glass slides (25mm×75mm×1mm) were obtained from VWR (West Chester, PA). Sodium bicarbonate (NaHCO3) (all reagent grade), 6-mercapto-1-hexanol (MCH), tris-(2-carboxyethyl) phosphine hydrochloride (TCEP) were purchased from Sigma-Aldrich (St. Louis, MO); Methylene Blue (MB), carboxylic acid, succinimidyl ester (MB-NHS) from Biosearch Technologies, INC, (Novato, CA).Poly(dimethylsiloxane) (PDMS) was acquired from Dow Corning (Midland, MI). U937 cells were purchased from ATCC (Manassas, VA). All chemicals were used without further purification. The 28-mer TNF-α-binding aptamer sequence was synthesized as follows: 5'/5AmMC6/rG*rG*rA*rG*rU*rA*rU*rC*rU*rG*rA*rU*rG*r A*rC*rA*rA*rU*rU*rC*rG*rG*rA*rG*rC*rU*rC*rC/3ThioMC 3-D/-3' (IDT Technologies, San Diego, CA). Phosphorothioates (or S-oligos, marked with *) were used to stabilize RNA against RNase degradation. The aptamer was further modified at the 3-terminus with a C6-disulfide [HO(CH2)6-S-S-(CH2)6-] linker for surface immobilization, and the 5-end was modified with an amine group for redox probe (i.e. MB) conjugation. The aptamers were dissolved in 1× PBS buffer (pH 7.4).

Conjugation of Methylene Blue Redox Moiety to the TNF-α Aptamer

To attach the methylene blue redox molecule to the 3' end of the aptamer, the protocol reported previously was followed[25]. Briefly, TNF-α aptamer stock solution was stored as 100μM, 50μL aliquots. To attach methylene blue molecules to the 5' end of the aptamer, 0.3mg of MB-NHS (a large concentration) was added to 20μL of dimethyl formamide, followed by 20μL of PBS and 10μL of 0.5M NaCO3 buffer for maintaining a pH of 8.3.The amine-reactive NHS ester from the redox probe links to the terminal amine group of the aptamer. The solution was kept at 4˚C for 4 h to allow the chemicals to react, and then it was stored at -20˚C until ready for use.

Electrochemical Measurements and Sensor Calibration

Calibration curves were measured by challenging the aptasensor with different concentrations of TNF-α ranging from 1 to 200ng/mL, dissolved in RPMI 1640 media. TNF-α was allowed to bind to the sensor for 30min before acquiring a signal. Signals were measured using square wave voltammetry (SWV) using a potentiostat (CHI842b, CH Instruments, Austin, TX), scanning from -0.5V to 0V with 0.004V increments, 0.04V amplitude, and 60Hz frequency. Peak heights were determined either by using the software from CH Instruments or through a peak-finding script written in Python.

Fabrication of Micropatterned Gold Electrodes

The electrode layout was designed in AutoCAD and a 20K photomask was printed by CAD/Art services (Bandon, Oregon).Standard photolithography and metal etching techniques were used to micropattern the gold electrodes as described previously[31]. A 150Å layer of chrome and 1000Å layer of gold were sequentially sputtered onto glass microscope slides (25mm x 75mm x 1mm) by LGA Thin Films (Santa Clara, CA).Note that the photoresist layer was not immediately removed but remained to protect the gold electrodes from the subsequent silane modification. The gold and chrome layers were etched to form a 2-by-4 array of circular electrodes, 300μm in diameter. The electrodes were connected via 20μm leads to 2mm x 2mm contact pads located on the edges of the glass substrate. To reliably attach the gold contact pads to a computer-controlled multiplexer (NI ER-16, National Instruments, TX), contact strips were patterned from copper-clad printed circuit board (PCB) (Radio Shack, Fort Worth, TX).The copper strips were kept in contact with the contact pads using miniature C-clamps, and wires were soldered at the other end of the strip and connected to the multiplexer.

Microfluidic Chamber Feature Design and Fabrication

The microchamber and flow channel height is 100μm, the standard height of our microfluidic features, to allow for steady flow rates via decreased fluidic resistance[30].

Poly(dimethylsiloxane) (PDMS) devices were fabricated using standard soft lithography (SU-8) procedures[32]. SU-8 2050 (Microchem, Newton, MA) was spincoated according to the provided spin curves onto a 4" test-grade silicon wafer (University Wafer, South Boston, MA) for 100μm feature heights. Feature heights were validated using a Digital Linear gauge with 1μm resolution (EG-225, Ono Sokki, Addison, IL). Features were patterned by exposing UV light through a 20K photomask (CAD/Art Services, Bandon, OR), and areas of exposed SU-8 would crosslink and become impervious to the SU-8 developer. PDMS was poured onto the featured silicon wafer, degassed in a vacuum chamber, and baked at 70˚C for 1.25h.To create the two-layered device, a protocol similar to the one developed by Eddings and co-workers was used[33]. The thick control layer (top, 5:1 elastomer to curing agent), entered the oven for 20 min ahead of the thin flow layer (bottom, 20:1 elastomer to curing agent).After baking the control layer for one hour, the devices were taken out of the oven, cut out, and holes for the vacuum line were punched using a 16 gauge needle (BD Falcon, Franklin Lakes, New Jersey). When these devices were fully prepared, the bottom layer was taken out of the oven and the two layers were aligned according to fiduciary marks under a microscope. Upon baking the devices in the oven for an additional 20min, the devices were cut out and the holes for the flow layer were punched. The last bake step aids in curing and bonding the two layers of PDMS together, minimizing delamination and device failure.

PEG Patterning for Defining Cell-Capture Sites

Glass substrates featuring photoresist-protected patterned gold microelectrodes were modified with an acryl silane process detailed previously in order to covalently bind PEG molecules to the substrate[34]. Upon completion of the silane modification, the electrodes were sonicated for 5min in acetone and then baked at 100˚C for 3h to fully crosslink the silane layer[35]. To define cell-capture areas, a PEG prepolymer solution containing PEG-diacrylate (PEG-DA, MW 575) and 2% (v/v) photoinitiator was spin-coated onto the acryl-modified substrate at 800rpm for 4s. A photomask was aligned to the patterned electrodes using fiduciary marks visualized through a Canon PLA-501F mask aligner. Upon exposure to 60mJ/cm2 UV light (Omnicure Series 1000, Lumen Dynamics, Mississauga, Ontario, Canada) for 1s, areas unprotected by the photomask underwent radical polymerization and cross-linked into a gel. Conversely, the PEG prepolymer in protected, unexposed areas were removed by immersing the substrate in deionized water for 5min. This strategy enables us to control cell-capture areas since PEG exhibits non-fouling properties while the unexposed areas retain active acryl silane groups, allowing for subsequent physical adsorption of antibodies.

Preparation of Microdevices and Cell Experiments

After fabricating PEG wells on the patterned gold substrates, 0.5μL of 10μM MB-conjugated thiolated aptamer solution was pipetted onto each electrode an incubated in a humidified, dark environment for 1h, allowing for SAM assembly via a gold-thiol reaction. Upon gentle rinsing in DI water, a subsequent incubation of 1μM MCH for 15min was used to correct any inappropriately-bound aptamers (e.g. aptamers bound by physical adsorption as opposed to a gold-thiol bond), promoting a more specific signal. Next, the MCH solution was likewise gently rinsed away and a 0.5μL solution containing CD4 antibodies at 0.2mg/mL was pipetted onto each cell capture region and incubated for 1h, allowing the antibodies to be physisorbed onto the exposed silane areas only.

Afterward, the PDMS devices were aligned to the glass substrate under a microscope such that the chambers enclosed alternating PEG wells and electrodes. The PDMS device was adhered to the glass substrates by applying a vacuum to a spiderweb feature surrounding the device as reported by Schaff and co-workers[36]. When introducing liquids into the flow channel, the vacuum was applied to the control layer, raising the chambers and facilitating fluid flow into the entire microchannel.

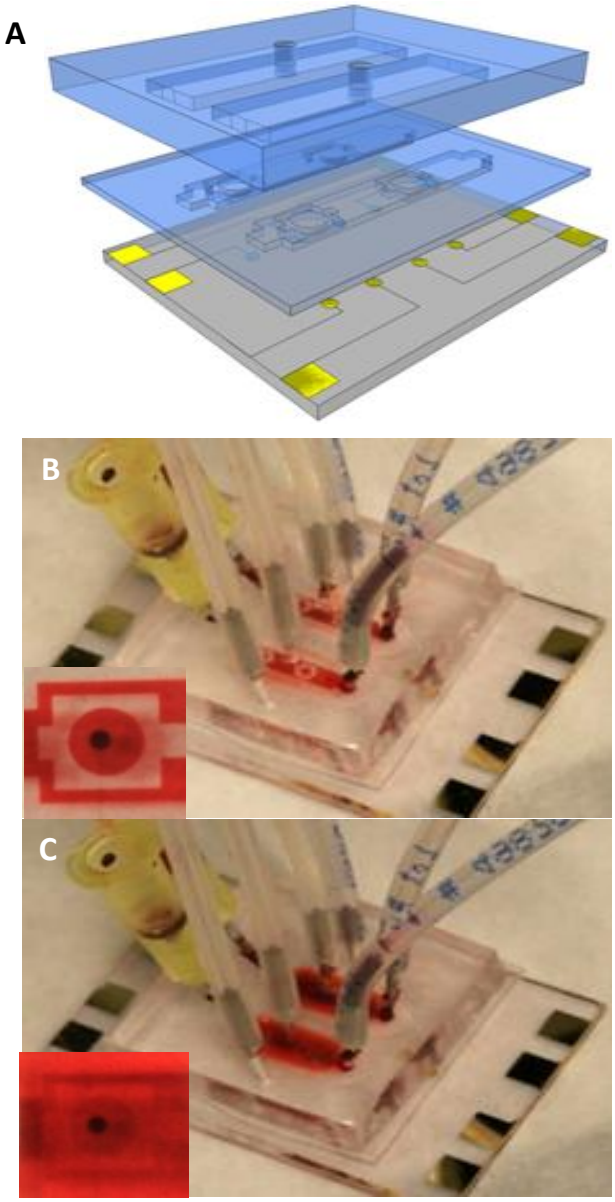

Figure 2. Reconfigurable microfluidic devices. (**A**) Exploded view of device components showing two layers of PDMS assembled onto a glass slide with micropatterned gold electrodes. (**B-C**) Microfluidic devices infused with food dye to demonstrate chamber actuation. In the collapsed configuration, the walled structures collapse and the chambers become macroscopically visible – white rings are the walls of microchambers (B). Upon applying vacuum the microchambers are raised and the food dye becomes uniforms distributed throughout the channel (C)

Microdevice to Study Paracrine Interactions

The microfluidics were designed such that one group of cells could be protected by the chamber while a neighbouring group of cells could remain exposed to the bulk environment of the microfluidic channel. To enhance cell functionality, experiments were conducted at 37°C using a heating stage. After priming the channel with 1x PBS, the channel was rinsed with serum-free RPMI 1640 without phenol red, and media-containing U937 cells (10^6cells/mL) were flowed into the channel. Cells were given 30min to bind to the antibodies, and any unbound cells were subsequently rinsed away at a flow rate of 20µL/min. Upon immobilizing U937 cells around each cell capture/electrode region, media containing PMA/Ionomycin (81nM and 1.34µM respectively) was infused into the channel, after which the micro-cups were deployed, trapping mitogenic stimulant around the enclosed group of cells. In the meantime, the microfluidic channel was flushed with fresh RPMI to minimize exposure of the other group of U937 cells to the mitogen. The short term exposure did not appreciably stimulate the cells in the open channel while the neighbouring cells confined to the micro-cups became activated. The cells were incubated with mitogens inside the micro-cups for 60min. TNF-α signal was monitored both inside the micro-cup and from quiescent cells using an automated multiplexer and potentiostat. Once the micro-cups were lifted, a 0.1µL/min flow rate was applied to allow for convection of cytokines from the activated to quiescent cells. Electrochemical measurements were made as described before to quantify local TNF-α concentration at each group of cells.

A separate experiment was carried to exclude the possibility that an increase in TNF-α signal next to quiescent cells was due to convention only from the upstream group of cells and did not involve endogenous cytokine production by these cells. To verify this, we developed a protocol of capturing and stimulating U937 cells around the upstream electrode only. By selectively incubating CD4 antibodies around the chambered electrodes, cells would only attach to these upstream electrodes. Rinsing at 20µL/min removed any non-specifically bound cells. The cells were stimulated with PMA/Ionomycin as described previously, and the local concentration of downstream TNF-α was monitored by SWV.

A final experiment was performed where the downstream cells were pre-treated with 10ng/mL interleukin (IL)-10, an anti-inflammatory cytokine, for 16h prior to experiment. IL-10 treated cells were seeded while the upstream chambers were collapsed, preventing these cells from being seeded upstream. After rinsing unbound pretreated cells, the chambers were raised and untreated cells were captured around the upstream electrode. These cells were likewise stimulated with PMA/Ionomycin and local TNF-α production was measured using SWV. Additional details may be found in the Supplementary Information Part 4.

Results and Discussion

Microfluidic Device Actuation

Microstructured membranes deployed inside microfluidic channels offer unique advantages in terms of entrapment of cells and analysis of cellular contents[37-41]. The goal of this study was to incorporate aptasensors for cell analysis reported by us previously[25, 29] into reconfigurable microfluidic devices. As shown in the schematic of Figure 1, the chambers were designed to cover alternating electrodes so that the effect of using the cups could be compared directly to a sensing area without a cup. Furthermore, this design facilitated cell-cell communication studies whereby a group of cells inside the microchamber could be exposed to a stimulant while rinsing a stimulant away from the channel. This strategy allowed the activation of a specific group of cells followed by monitoring its interactions with non-activated cells via TNF-α secretion. Figure 2A shows multiple layers comprising a microfluidic device. The devices were

engineered for raising and lowering the microstructured PDMS roof of the microfluidic channel by applying vacuum to features located directly above miniature electrodes and cell attachment sites. In its native state, the flow layer containing microchambers was lowered and the device walls were in contact with the glass substrate creating compartments for cell analysis. When applying vacuum, the fluid was uniformly distributed within the entire channel; however, upon releasing the vacuum, the fluid is sequestered into the 80nL microchambers (Figure 2B, 2C). Importantly, raising and lowering of the microchambers over the electrode did not affect sensor performance for at least 10 on/off cycles (Figure S1).

TNF-α Aptasensor Performance and Calibration Curve

TNF-α aptamer is an RNA molecule with G-rich regions and a likely hairpin structure[42]. This RNA molecule was further modified to enhance nuclease resistance[43] and labelled with a redox reporter, methylene blue (MB). The TNF-α hairpin aptamer was immobilized onto the gold electrode by modifying the 5'-end with a thiol group, creating a gold-thiol bond. The 3'-end is modified with a MB redox reporter such that in the hairpin state, the MB molecule remained close to the surface of the electrode and facilitated electron transfer[44]. Upon binding to the target protein, the aptamer hairpin unfolded decreasing the electron transfer efficiency between redox reporters MB and the electrode (Figure 3A). This resulted in TNF-α concentration dependent decrease of redox peak shown in Figure 3B.

Since the sensor generates smaller peak currents in the presence of cytokines, a so-called "signal-off" sensor, signals were calculated as a percentage of suppression. Time-series analysis was done by comparing the percentage change of the present signal with the signal strength at t=0, i.e. signal suppression(t) = (I(t) – I(0))/I(0).

To determine limit of detection and linear range, the aptasensor was challenged with increasing levels of recombinant TNF-α. The plot of change in peak current (signal suppression) vs. concentration (Figure 3C) shows that the limit of detection is 5ng/mL with sensor range extending to 100ng/mL. The limit of detection was calculated by taking the standard deviation of the signal from three consecutive SWV scans and multiplying it by three, providing a 99.7% confidence interval for any SWV scan. The result, 5.6% signal suppression, corresponded to a limit of detection of 5ng/mL. By referring to the calibration curve, the electrical signals could be correlated to concentrations of TNF-α.

Detecting Cell-Secreted TNF-α within Actuated Microchambers

Cells were infused into microfluidic devices and captured around micropatterned electrodes modified with TNF-α-specific aptamers (Figure 4A). In a typical experiment, ~600 cells were captured in the 800μm diameter PEG wells. Upon PMA/ionomycin stimulation, the vacuum for the control line was turned off, lowering the microstructured roof of the microfluidic device and confining cells/electrode within 80nL microchambers. The roof was microstructured such that one group of cells/electrode was in the open channel (Figure 4A, right electrode) while the neighbouring cells were enclosed in the microchamber (Figure 4A, left electrode).The system was monitored over four hours with signals collected at 15, 30, 60, 120, and 240 min.

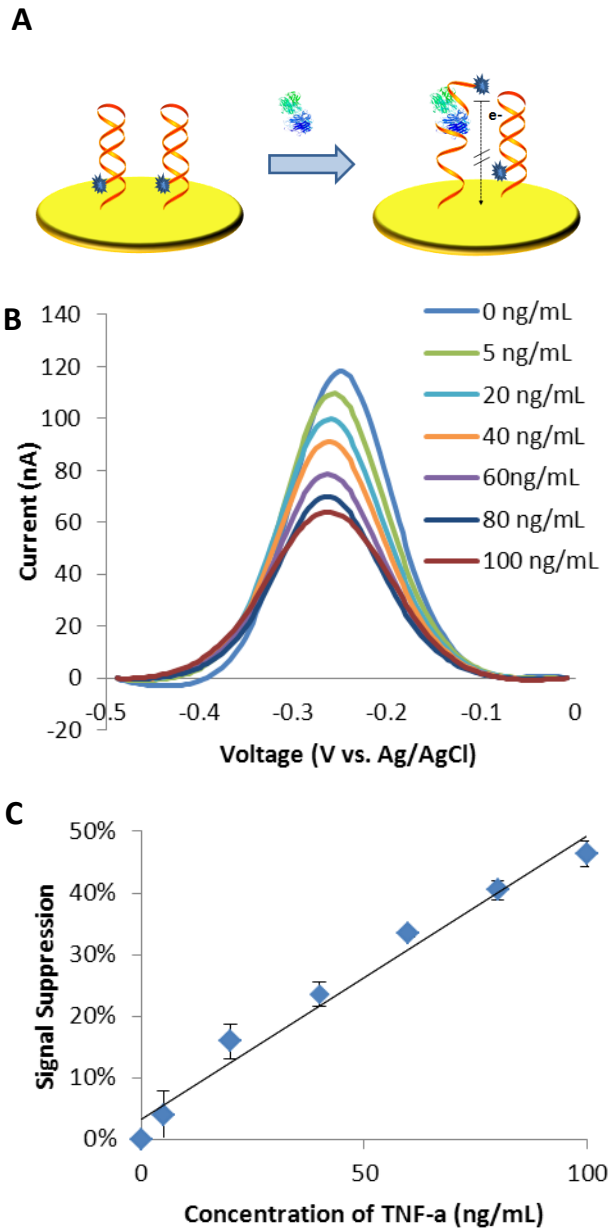

Figure 3. Sensor function and calibration. **(A)** The aptasensor was challenged varying concentrations of recombinant TNF-α and changes in electrode redox properties were quantified by SWV. **(B)** A calibration curve was constructed by plotting the percentage of signal lost (signal suppression) against the concentration. The limit of detection was 5ng/mL with linear range extending to 100 ng/mL. These data were fitted to a line whose equation is y = 0.004613x + 0.03311 with R^2 = 0.9768.The error bars represent the standard deviation of data acquired from at least three different electrodes for each concentration.

The results presented in Figures 4B for stimulated cells (and S2B for unstimulated cells) show that the utilization of microchambers improves response time and increases the overall signal strength as a result of increased local concentrations and decreased diffusion lengths. Within 30 min, 12.2% signal suppression was measured from stimulated U937 cells confined inside microchambers compared to 8.03% signal suppression measured from cells in the open configuration. At the 2h and 4h

time points, a 2 fold signal enhancement was observed in the case of the enclosed cells. One can note that in Figure 4B the signal approaches 60% signal suppression after 240min of stimulation. Based on the calibration data presented in Figure 3B this likely suggests saturation of the sensor surface as opposed to the attenuation in cytokine secretion rate.

In a validation experiment, glass surface containing hydrogel microwells of the same dimensions as discussed above were functionalized with antibodies for detection of TNF-α and capture of cells[45]. These micropatterned surfaces were integrated into reconfigurable microfluidic device and used to analyse TNF-α release from U937 cells. The secretion of TNF-α was revealed by staining micropatterned surfaces with secondary antibodies. As shown in Figure S3B, a 2.3 fold increase in fluorescence intensity was observed. This result compares well with and validates the electrochemical detection of TNF-α discussed in Figure 4.

To determine cell secretion rates, we constructed models for simulating cytokine production, diffusion, and binding in COMSOL (COMSOL Inc., Burlington, MA), and the simulation details can be found in the Supplemental Information (Figure S2, Table S1).From the model, the average cytokine production rate was determined to be 0.0243±0.0007pg/cell/hour for activated cells in an enclosed chamber, compared to 0.0174±0.0006pg/cell/hour in the open chamber, similar to the rates found in previous reports[29, 46-48].For quiescent cells, the rates were 0.0080±0.0004 for enclosed cells and 0.0036±0.0005pg/cell/hour in the open chamber.

While confinement of cells in a small volume of the microchamber was expected to limit diffusion and increase local concentration of TNF-α, the observation that confinement enhanced TNF-α secretion rate was less expected and more exciting. Figure 4B compares experimentally measured electrical enhancement from activated cells (solid line) to the signal enhancement that would be expected based on the decrease in chamber dimensions without the change in cell secretion rates. Thus, our results suggest that in addition to concentrating the cell-secreted cytokines, this device may also amplify the autocrine/paracrine effects of these cytokines. Additional computational models were run to verify that the signal increase is not an artefact of the constant rate assumption (Figure S2).

Using Reconfigurable Chambers to Monitor Communication Between Two Groups of Cells

U937 cells are monocyte-like cells that are known to not only secrete TNF-α but to also to become activated by TNF-α in a paracrine and autocrine fashion[49-52]. Thus, these cells provide a model system to study reciprocal interactions via the same secreted factor. Leveraging this fact, we wanted to set up a proof of concept experiment where a group of monocytes is stimulated to produce TNF-α while the neighboring group of cells remains unstimulated. The goal of this experiment was to monitor communication between active and quiescent cells vis-à-vis TNF-α signal.

As shown in Figure 4A cells around one electrode could be completely isolated from the external flow environment while cells around a separate electrode could remain exposed to the bulk solution. Upon flowing mitogenic stimulant into the channel, the chamber was lowered around the upstream electrode, incubating confined cells in stimulant while the stimulant in the

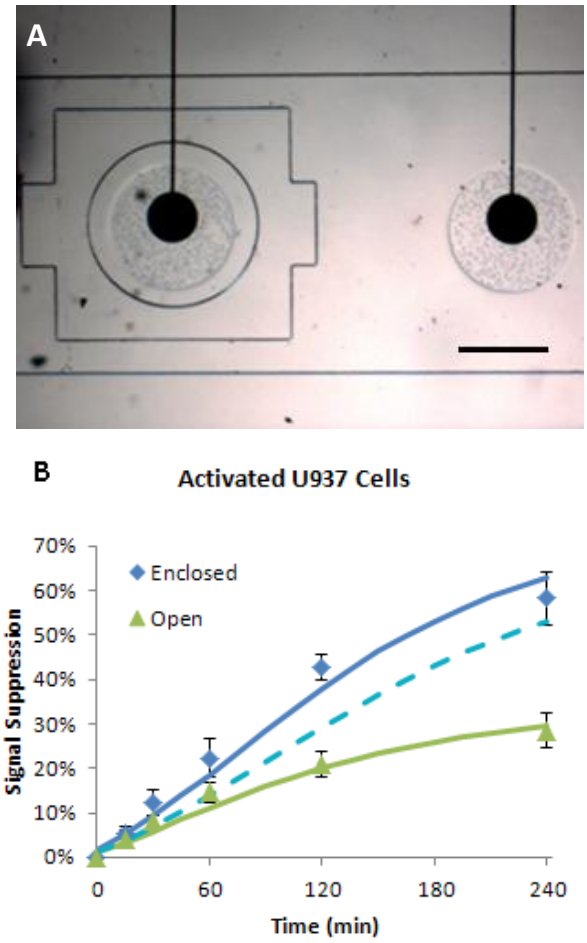

Figure 4. (A) Image demonstrating cell capture around the electrodes within microfluidic chambers. Note the two groups of cells; the group on the left is trapped inside an actuatable microchamber while the group on the right is placed in the open channel. Also note the circular electrodes connected with leads (appear black in the picture). Scale bar is 500µm. **(B)** Electrochemical detection of TNF-α secretion from monocytes (U937) inside the reconfigurable device over 4 h, with mitogenic activation (B) or without stimulation (Figure S3B).This experiment was performed using the configuration shown in (A) with both open and enclosed cells located in the same channel. The solid lines show simulated signal suppression profiles using the best fit constant secretion rate. The dashed lines show the expected secretion profile when applying the "open" secretion rate to the "closed" geometry, showing the expected increase due to the improved geometry alone. The additional difference implies paracrine signaling may play a role in the system, prompting a study for monitoring paracrine signaling via reconfigurable microfluidics.

bulk was rinsed away. After incubation for 1h, the inner chamber was raised and the device was subject to flow at 0.1 µL/min, allowing signals from upstream cells to convect towards downstream cells. As a control to determine the expected amount of cytokines detected at the downstream electrode, cells were patterned only around the upstream electrode. As shown in Figure 5A, TNF-α signal was concurrently measured in two locations inside a microfluidic channel: 1) near mitogen-activated monocytes upstream and 2) near quiescent monocytes downstream. As noted above, TNF-α is an autocrine/paracrine stimulus for monocytes and we expected quiescent monocytes to become TNF-α producers after being exposed to activated monocytes located upstream. Figure 5B summarizes experimental

results from different devices, with n=5 for communication experiments and n=3 for convection experiments. As seen from these results, during the 1st hour, a group of cells immersed in the mitogen solution inside a closed chamber is producing high levels of TNF-α (measured by the upstream electrode, Figure 5B pink diamonds) while the other group of cells inside the open channel where mitogen was carefully flushed out remains relatively quiescent (downstream electrode, Figure 5B blue circles). Once the chamber confining/isolating activated monocytes is raised and the microchannel is subject to flow, the signal at the downstream electrode begins to increase. This increase in signal combines diffusion/convection of TNF-α from the upstream location with production of TNF-α by the previously quiescent cells located downstream. We therefore carried out control experiments with cells patterned only around the upstream electrode. As seen from Figure 5B, after stimulation of the cells around the upstream electrode, raising of the microchamber, and flowing TNF-α downstream, the electrical signal at the downstream electrode (green triangles) increased but not to the level that was observed when cells were present at the downstream location. This control experiment helped identify the fraction of the signal attributable to endogenous TNF-α produced by the downstream cells as opposed to exogenous cytokine molecules originating from a different location. Statistical analysis of the data revealed that at the 154 minute timepoint (88 minutes after commencing cross-talk between two groups of cells), data from the downstream electrode with cells becomes significant compared to the convection data (t-test, $p<0.05$). It is not unreasonable that secondary stimulation in the cells located downstream did not result in the same level of activation as the primary stimulation of cells located upstream. It is likely that mitogenic activation experienced by the cells located upstream elicits a much stronger cytokine response than the autocrine/paracrine stimulation experienced by the downstream cells[49].

To further highlight that the cellular cross-talk is indeed occurring, we set up another experiment where one group of cells located at the upstream electrode was activated as before but the other group of cells was pre-treated with an anti-inflammatory cytokine interleukin (IL)-10. Pre-treatment with this cytokine was expected to render the cells less likely to be activated by inflammatory signals such as TNF-α[53, 54]. As seen by the red square profile in Figure 5B this was indeed the case, with downstream cells remaining relatively quiescent, even in the presence of TNF-α signals diffusing from the upstream location of activated cells. Further details may be found in the Supplementary Information Figure S4. This experiment demonstrates once again the flexibility afforded by the microsystem to modulate phenotype of one group of cells and to monitor its communication with another group of cells located a short distance away.

Conclusions

This paper demonstrates the utility of reconfigurable, vacuum-actuated microfluidic chambers with integrated aptasensors for local and dynamic detection of TNF-α release from cells. One use of such a microsystem highlighted here is in monitoring paracrine cross-talk between groups of cells. To prove the concept, we monitored two groups of immune cells communicating via secreted TNF-α. We observed 1) release of TNF-α from one group of cells, 2) its diffusion/convection to the downstream location in the microchannel containing quiescent cells and 3) Given that paracrine, reciprocal interactions between different groups of cells are ubiquitous in cancer, development biology, immunology and tissue injury, the microsystem described here may have applications for dissecting intercellular communication. It may serve as a valuable tool for improving understanding of how specific cell types contribute to the milieu of signals produced during injury or inflammation and for testing cell type-specific therapies aimed at attenuating effects of inflammation or injury.

Acknowledgements

This work was supported by NSF EFRI Grant No. 0937997 awarded to AR. TK was supported by NIH Fellowship T32 - NIBIB 5T32EB003827. Additional funding came from "Research Investments in Science and Engineering from UC Davis".

[a]*Department of Biomedical Engineering, University of California, Davis, Genome and Biomedical Sciences Building, 451 Health Sciences Drive Room 2619, Davis , CA 95616, United States.Tel: (530) 792-2383; E-mail: arevzin@ucdavis.edu*

† Electronic Supplementary Information (ESI) available: [Supplementary_Information.pdf] See DOI: 10.1039/b000000x/

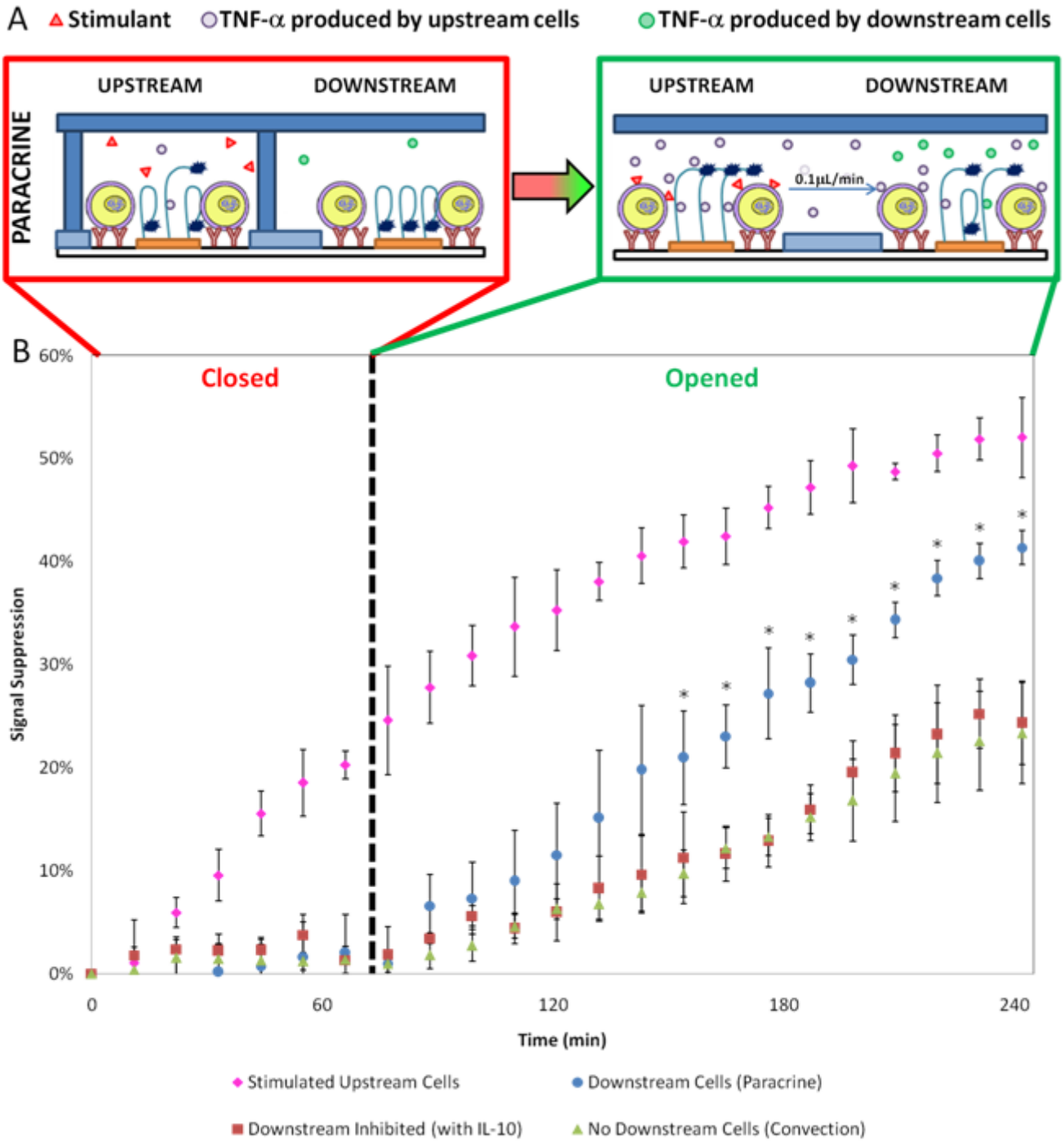

Figure 5. Monitoring cellular cross-talk using reconfigurable microfluidic devices. (A) Schematic of the experiments. Cells around upstream electrode were confined inside the microchamber and stimulated with a mitogen while cells in the open channel around downstream electrode were not activated. At the 66 min time point the microchamber was raised and the communication between activated and quiescent monocytes was monitored vis-à-vis TNF-α. In a control experiment, only one group of cells was used. These cells were captured around only the upstream electrode and stimulated as discussed above; no cells were present at the downstream electrode. These experiments were designed to account for convection/diffusion from activated cells and to help bring to the fore TNF-α signal produced by the downstream cells. (B) TNF-α secretions were monitored every 11 min and differed significantly between "Paracrine" and "Convection" at timepoints beginning at 154min (T test, $p < 0.05$, denoted by *), 88 min after raising the chambers and commencing interaction between active and inactive monocytes. An additional experiment showed that cells pretreated with IL-10 were not responsive to upstream TNF-α signals, depicted by red squares. Error bars represent ±1σ.

Notes and references

1. I. A. Clark, *Cytokine Growth F R*, 2007, 18, 335-343.
2. R. van Horssen, T. L. M. ten Hagen and A. M. M. Eggermont, *Oncologist*, 2006, 11, 397-408.
3. M. Feldmann and R. N. Maini, *Annual review of immunology*, 2001, 19, 163-196.
4. S. L. Waldrop, C. J. Pitcher, D. M. Peterson, V. C. Maino and L. J. Picker, *The Journal of clinical investigation*, 1997, 99, 1739-1750.
5. M. R. Amel Kashipaz, D. Swinden, I. Todd and R. J. Powell, *Clinical and experimental immunology*, 2003, 132, 360-365.
6. C. C. Czerkinsky, L.-Å. Nilsson, H. Nygren, Ö. Ouchterlony and A. Tarkowski, *Journal of Immunological Methods*, 1983, 65, 109-121.
7. S. Tanguay and J. J. Killion, *Lymphokine and cytokine research*, 1994, 13, 259-263.
8. D. G. Ginzinger, *Exp Hematol*, 2002, 30, 503-512.
9. P. Stordeur, L. F. Poulin, L. Craciun, L. Zhou, L. Schandene, A. de Lavareille, S. Goriely and M. Goldman, *Journal of Immunological Methods*, 2002, 262, 229-229.
10. R. C. Bailey, G. A. Kwong, C. G. Radu, O. N. Witte and J. R. Heath, *Journal of the American Chemical Society*, 2007, 129, 1959-1967.
11. R. Fan, O. Vermesh, A. Srivastava, B. K. Yen, L. Qin, H. Ahmad, G. A. Kwong, C. C. Liu, J. Gould, L. Hood and J. R. Heath, *Nature biotechnology*, 2008, 26, 1373-1378.
12. G. Stybayeva, O. Mudanyali, S. Seo, J. Silangcruz, M. Macal, E. Ramanculov, S. Dandekar, A. Erlinger, A. Ozcan and A. Revzin, *Analytical chemistry*, 2010, 82, 3736-3744.
13. H. Zhu, G. Stybayeva, M. Macal, E. Ramanculov, M. D. George, S. Dandekar and A. Revzin, *Lab Chip*, 2008, 8, 2197-2205.
14. J. C. Love, J. L. Ronan, G. M. Grotenbreg, A. G. van der Veen and H. L. Ploegh, *Nature biotechnology*, 2006, 24, 703-707.
15. C. M. Story, E. Papa, C. C. Hu, J. L. Ronan, K. Herlihy, H. L. Ploegh and J. C. Love, *Proceedings of the National Academy of Sciences of the United States of America*, 2008, 105, 17902-17907.
16. N. Hashemi, J. S. Erickson, J. P. Golden and F. S. Ligler, *Biomicrofluidics*, 2011, 5, 32009-320099.
17. A. Jin, T. Ozawa, K. Tajiri, T. Obata, S. Kondo, K. Kinoshita, S. Kadowaki, K. Takahashi, T. Sugiyama, H. Kishi and A. Muraguchi, *Nature medicine*, 2009, 15, 1088-1092.
18. S. Yamamura, H. Kishi, Y. Tokimitsu, S. Kondo, R. Honda, S. R. Rao, M. Omori, E. Tamiya and A. Muraguchi, *Analytical chemistry*, 2005, 77, 8050-8056.
19. H. Zhu, G. Stybayeva, J. Silangcruz, J. Yan, E. Ramanculov, S. Dandekar, M. D. George and A. Revzin, *Analytical chemistry*, 2009, 81, 8150-8156.
20. A. M. Clark, K. M. Sousa, C. N. Chisolm, O. A. MacDougald and R. T. Kennedy, *Analytical and bioanalytical chemistry*, 2010, 397, 2939-2947.
21. Q. Han, N. Bagheri, E. M. Bradshaw, D. A. Hafler, D. A. Lauffenburger and J. C. Love, *Proceedings of the National Academy of Sciences of the United States of America*, 2012, 109, 1607-1612.
22. G. Stybayeva, M. Kairova, E. Ramanculov, A. L. Simonian and A. Revzin, *Colloids and surfaces. B, Biointerfaces*, 2010, 80, 251-255.
23. T. Endo, S. Yamamura, K. Kerman and E. Tamiya, *Analytica chimica acta*, 2008, 614, 182-189.
24. M. S. Luchansky and R. C. Bailey, *Analytical chemistry*, 2010, 82, 1975-1981.
25. Y. Liu, N. Tuleouva, E. Ramanculov and A. Revzin, *Analytical chemistry*, 2010, 82, 8131-8136.
26. J. J. Li, X. Fang and W. Tan, *Biochemical and biophysical research communications*, 2002, 292, 31-40.
27. N. Hamaguchi, A. Ellington and M. Stanton, *Analytical biochemistry*, 2001, 294, 126-131.
28. Y. Xiao, B. D. Piorek, K. W. Plaxco and A. J. Heeger, *Journal of the American Chemical Society*, 2005, 127, 17990-17991.
29. Y. Liu, T. Kwa and A. Revzin, *Biomaterials*, 2012, 33, 7347-7355.
30. Y. Liu, J. Yan, M. C. Howland, T. Kwa and A. Revzin, *Analytical chemistry*, 2011, 83, 8286-8292.
31. J. Yan, V. A. Pedrosa, A. L. Simonian and A. Revzin, *Acs Appl Mater Inter*, 2010, 2, 748-755.
32. M. A. Unger, H. P. Chou, T. Thorsen, A. Scherer and S. R. Quake, *Science*, 2000, 288, 113-116.
33. M. A. Eddings, M. A. Johnson and B. K. Gale, *Journal of Micromechanics and Microengineering*, 2008, 18, 067001.
34. A. Revzin, R. G. Tompkins and M. Toner, *Langmuir*, 2003, 19, 9855-9862.
35. J. Kim, G. J. Holinga and G. A. Somorjai, *Langmuir*, 2011, 27, 5171-5175.
36. U. Y. Schaff, M. M. Q. Xing, K. K. Lin, N. Pan, N. L. Jeon and S. I. Simon, *Lab Chip*, 2007, 7, 448-456.
37. D. Irimia, R. G. Tompkins and M. Toner, *Analytical chemistry*, 2004, 76, 6137-6143.
38. C. Ma, R. Fan, H. Ahmad, Q. Shi, B. Comin-Anduix, T. Chodon, R. C. Koya, C. C. Liu, G. A. Kwong, C. G. Radu, A. Ribas and J. R. Heath, *Nature medicine*, 2011, 17, 738-743.
39. Y. Gao, D. Majumdar, B. Jovanovic, C. Shaifer, P. C. Lin, A. Zijlstra, D. J. Webb and D. Li, *Biomedical microdevices*, 2011, 13, 539-548.
40. Q. Meng, Z. He, L. Zhang, L. Zhao, E. Li, Q. Zhang, X. Zhang, D. Yang, L. Zou, Z. Gao and Q. Wang, *Electrophoresis*, 2011, 32, 3446-3453.
41. A. Chen, T. Vu, G. Stybayeva, T. R. Pan and A. Revzin, *Biomicrofluidics*, 2013, 7.
42. Y. Liu, Q. Zhou and A. Revzin, *The Analyst*, 2013, 138, 4321-4326.
43. C. Wilson and A. D. Keefe, *Current opinion in chemical biology*, 2006, 10, 607-614.
44. R. J. White, N. Phares, A. A. Lubin, Y. Xiao and K. W. Plaxco, *Langmuir*, 2008, 24, 10513-10518.
45. J. H. Seo, L. J. Chen, S. V. Verkhoturov, E. A. Schweikert and A. Revzin, *Biomaterials*, 2011, 32, 5478-5488.
46. E. C. Hulme and M. A. Trevethick, *British journal of pharmacology*, 2010, 161, 1219-1237.
47. M. S. Kim, S. H. Lee, M. Y. Song, T. H. Yoo, B. K. Lee and Y. S. Kim, *Journal of molecular biology*, 2007, 374, 1374-1388.
48. B. Scallon, A. Cai, N. Solowski, A. Rosenberg, X. Y. Song, D. Shealy and C. Wagner, *The Journal of pharmacology and experimental therapeutics*, 2002, 301, 418-426.
49. S. A. Rushworth, S. Shah and D. J. MacEwan, *J Immunol*, 2011, 187, 702-707.
50. S. Heidenreich, M. Weyers, J. H. Gong, H. Sprenger, M. Nain and D. Gemsa, *J Immunol*, 1988, 140, 1511-1518.
51. D. M. Smith, G. A. Lackides and L. B. Epstein, *Cancer research*, 1990, 50, 3146-3153.
52. P. A. Baeuerle and T. Henkel, *Annual review of immunology*, 1994, 12, 141-179.
53. J. Rajasingh, E. Bord, C. Luedemann, J. Asai, H. Hamada, T. Thorne, G. Qin, D. Goukassian, Y. Zhu, D. W. Losordo and R. Kishore, *FASEB journal*, 2006, 20, 2112-2114.
54. A. Denys, I. A. Udalova, C. Smith, L. M. Williams, C. J. Ciesielski, J. Campbell, C. Andrews, D. Kwaitkowski and B. M. Foxwell, *Journal of immunology*, 2002, 168, 4837-4845.